The Single-Molecule Conductance and Electrochemical Electron-Transfer Rate Are Related by a Power Law

Emil Wierzbinski,[†] Ravindra Venkatramani,[‡,∥] Kathryn L. Davis,[†] Silvia Bezer,[§] Jing Kong,[§] Yangjun Xing,[⊥] Eric Borguet,[⊥] Catalina Achim,[§,*] David N. Beratan,[*,‡] and David H. Waldeck[†,*]

[†]Department of Chemistry, University of Pittsburgh, Pittsburgh, Pennsylvania 15260, United States, [‡]Departments of Chemistry, Physics, and Biochemistry, Duke University, Durham, North Carolina 27708, United States, [§]Department of Chemistry, Carnegie Mellon University, Pittsburgh, Pennsylvania 15213, United States, [⊥]Department of Chemistry, Temple University, Philadelphia, Pennsylvania 19122, United States, and [∥]Department of Chemical Sciences, Tata Institute of Fundamental Research, Homi Bhabha Road, Colaba, Mumbai 400 005, India

ABSTRACT This study examines quantitative correlations between molecular conductances and standard electrochemical rate constants for alkanes and peptide nucleic acid (PNA) oligomers as a function of the length, structure, and charge transport mechanism. The experimental data show a power-law relationship between conductances and charge transfer rates within a given class of molecules with the same bridge chemistry, and a lack of correlation when a more diverse group of molecules is compared, in contrast with some theoretical predictions. Surprisingly, the PNA duplexes exhibit the lowest charge-transfer rates and the highest molecular conductances. The nonlinear rate—conductance relationships for structures with the same bridging chemistries are attributed to differences in the charge-mediation characteristics of the molecular bridge, energy barrier shifts and electronic dephasing, in the two different experimental settings.

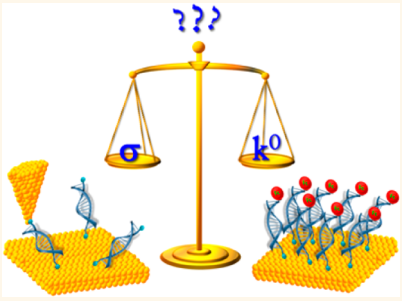

KEYWORDS: break junction · molecular bridge · charge transport · dephasing · nucleic acids

The propensity of molecules to transmit charge can be probed experimentally by measuring unimolecular charge-transfer rate constants, standard electrochemical rate constants, and molecular conductances. Unimolecular charge-transfer across a bridge (B) is typically measured by appending electron donor (D) and acceptor (A) groups to create a supermolecule (D-B-A), in which the charge transfer between the discrete electronic states of the donor and acceptor is triggered by a light flash and monitored by transient spectroscopy. In electrochemical charge transfer, charge flows between discrete electronic state(s) localized on the molecule to/from a high density of electrode electronic states. In molecular conductance measurements, the molecular bridge links two electrodes, each containing a large density of electronic states. Notwithstanding differences in experimental setups (*e.g.*, solvation, external electric fields, donor-acceptor electronic states), all three types of measurements described above report the charge transmission characteristics of the intervening molecular bridge. Thus, if the electronic structure of the molecular bridge is identical in the three experimental setups (*i.e.*, the different conditions in the experiments does not significantly affect the transmission characteristics of the bridge), one intuitively expects that the (zero-bias) molecular conductance, the electrochemical rate constant, and the unimolecular charge-transfer rates will be correlated. However, a quantitative evaluation of the relationship among rates and conductances is challenging to develop because neither the free energy of the reaction nor the reorganization energy are the same for the different measurements. If these two quantities can be controlled, or held constant, then measurements on a homologous series of molecular bridges can be compared and used to discern how the electronic coupling changes for different classes of measurements. Indeed, each of these quantities influences the bridge-mediated electronic coupling and the charge transfer kinetics.[1] The experimental studies

* Address correspondence to achim@cmu.edu, david.beratan@duke.edu, dave@pitt.edu.

Received for review March 15, 2013 and accepted May 21, 2013.

Published online 10.1021/nn401321k

reported here compare the electrochemical charge-transfer rate constant k^0 and the molecular conductance G for chemically identical molecular bridge units.

Prior theoretical studies predicted a correlation between molecular conductances and charge-transfer rates. A decade ago, Nitzan proposed a linear relationship between the unimolecular charge-transfer rate for donor-bridge-acceptor (D-B-A) molecules and the molecular conductance measured in metal-bridge-metal (M-B-M) junctions for superexchange transport.[2] That proposal stems from the similarities between the expressions for the nonadiabatic donor−acceptor charge-transfer rate k_{DA} and the near-zero bias Landauer conductance across a molecular junction g_{MJ}, derived assuming weak nearest neighbor couplings between the donor/acceptor/electrodes and the molecular bridge;[2] namely,

$$k_{DA} = \frac{2\pi}{\hbar}|V_{DB}V_{AB}|^2|G_B|^2F \quad (1)$$

and

$$g_{MJ} = \frac{e^2}{\pi\hbar}\Gamma_{LB}\Gamma_{RB}|\bar{G}_B|^2 \quad (2)$$

Here V represents the electronic couplings between the charge donor (D)/acceptor (A) and the molecular bridge (B). The coupling between the two electrodes (L and R) and the bridge is given by Γ. F is the Franck−Condon weighted density of states, which in the Marcus high temperature rate expression depends on the reaction free energy and the reorganization energy. The Green's functions of the molecular bridge in the rate and conductance expressions, G_B and $\bar{G}_B$, are different because in the latter case the bridge is coupled to a continuum of electrode states, which can shift and broaden the electronic states of the bridge. In the limit that the effect of the electrode on the molecular bridge is negligible, one can take $G_B \sim \bar{G}_B$ (the bridge is the same in the conductance and charge transfer setups) and write $g_{MJ} \propto k_{DA}$. This analysis was subsequently extended to treat hopping charge transfer.[3] Nitzan showed that the linear correlation between charge transfer rates and molecular conductances is preserved for a large number of bridging units, provided that the tunneling barrier is sufficiently large. Berlin and Ratner extended the hopping charge-transfer treatment to more general bridge models, while retaining the high-barrier condition.[4] In an alternative approach, Lewis and co-workers related nonadiabatic charge-transfer rates in D-B-A molecules and metal-bridge-acceptor (M-B-A) electrochemical systems to M-B-M molecular conductance junctions.[5] These four theoretical approaches[2−5] predict a linear relation between charge-transfer rates and molecular conductances in the superexchange regime and in the hopping regime, assuming high barriers compared to k_BT.

Do experimental rate data satisfy the predictions of these models? Lewis and co-workers applied their expressions to alkane and oligophenylethylene bridge data and found a correlation among molecular resistances (based on charge-transfer rates) and the inverse of the experimental conductance.[5] Amatore and co-workers[6] recently studied the rate-constant/conductance relationship for six molecules in the superexchange regime. They found that high-conductance molecules had large electrochemical charge-transfer rates. Here, the experimental values of k^0 for ferrocene-labeled PNA self-assembled monolayers (SAMs) are compared with the single-molecule conductances G of PNAs (with the same sequence) that we measure by STM-BJ experiments.[7] These data for PNA are combined with rate-conductance experimental data reported earlier for alkane[8,9] and DNA[10,11] bridges to provide a quantitative examination of the correlation between electrochemical charge-transfer rates and STM-BJ conductances. The data are examined as a function of the bridge length, chemical structure, and the charge-transfer mechanism (superexchange or hopping).

The rates and conductances vary considerably over the sequences of the single stranded (ss) and double stranded (ds) PNA used in our experiments. Our earlier studies indicated that charge transfer through PNA is hole mediated and can occur by tunneling or hopping, depending on the length, sequence, and strand hybridization (single *versus* double stranded PNA).[12−16] In particular, experiments focused on the presence of a guanine nucleobase in the nucleic acid sequence.[10,17−20] A nucleobase with oxidation potential lower than others in the sequence can stabilize positive charges (holes), lower the barrier for hole injection/tunneling, and thus facilitate charge transport.[21] Hence, charge-transfer rates can be enhanced by increasing the guanine content of a nucleic acid or by replacing adenine in thymine-adenine (TA) base pairs with 7-deazaadenine[19] or diaminopurine.[18,19] Finally, charge transfer through nucleic acids can be limited by base pair (bp) mismatches,[22−26] abasic sites,[22] and methylated or oxidized nucleobases.[27] We explore the dependence of charge-transfer properties on (i) the length of the PNA (**7 bp TA** *versus* **10 bp TA**), (ii) the guanine content (**7 bp TA** *versus* **7 bp 1 GC** and **7 bp 2 GC**), and (iii) the presence of mismatches (**10 bp 4 GC$_{(AT)}$** *versus* **10 bp 4 GC$_{(AC)}$**); see Table 1. For the ss PNA with three to six thymines and the ds PNAs with seven or ten base pairs, the electrochemical charge-transfer rate constants k^0 were reported earlier.[14,15] Data (k^0 and G) for 7 bp duplexes and rate data (k^0) for 10 bp duplexes appear elsewhere.[15,16,28] The other conductance data for PNA are newly reported here.

RESULTS

Electrochemical Charge-Transfer Rate Constants. For electrochemical studies, duplexes are assembled on gold electrodes using cysteine (Cys) to bind one of the strands to the electrode. Ferrocene (Fc) is used as the redox reporter and it is attached to the other end of the

TABLE 1. Sequences of ss and ds PNAs[a]

PNA type	Sequence	Notation
ss PNA	Cys-Tn-X, n = 3-6	T_n
7 bp ds PNA	Cys-TTT TTT T-Y AAA AAA A-Z	7 bp TA
	Cys-TTT **G**TT T-Y AAA **C**AA A-Z	7 bp 1 GC
	Cys-AA**G** TT**G** T-Y TT**C** AA**C** A-Z	7 bp 2 GC
10 bp ds PNA	Cys-TTT TTT TTT T-Y AAA AAA AAA A-Z	10 bp TA
	Cys-T**C**A **C**TA **G**AT **G**-Y A**G**T **G**A*T* **C**TA **C**-Z	10 bp 4 $GC_{(AT)}$
	Cys-T**C**A **C**TA **G**AT **G**-Y A**G**T **G**A*C* **C**TA **C**-Z	10 bp 4 $GC_{(AC)}$

[a] For electrochemistry experiments: X = Y = Fc and Z = Lys. For STM-BJ experiments: Y = (no linker), and X = Z = Cys.

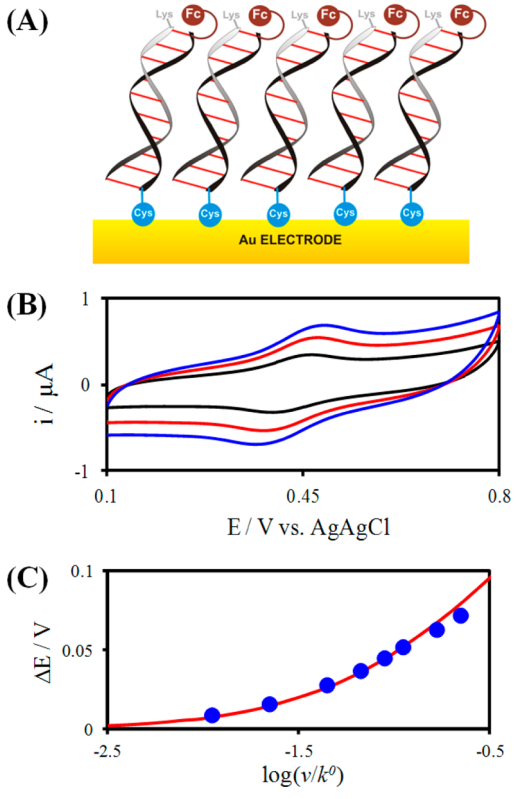

Figure 1. (A) Schematic representation of Fc-terminated PNA SAMs on gold electrodes used in cyclic voltammetry studies. (B) Voltammograms are shown for 7 bp 1 GC SAM measured in 1 M $NaClO_4$ solution at scan rates of 10 (black), 20 (red), and 30 (blue) mV/s. (C) Anodic peak potential shifts, ΔE are plotted *versus* the normalized scan rate (v/k^0) in which v is the scan rate and k^0 is the standard heterogeneous rate constant; the Marcus theory fit appears in red.

duplex, on the same strand that contains the Cys. Figure 1A shows a schematic representation of the ds

TABLE 2. Electrochemical Rate Constants k^0 for ds PNA SAMs

7 bp		10 bp	
sequence	k^0/s^{-1}	sequence	k^0/s^{-1}
TA	0.25 ± 0.05	TA	0.09 ± 0.02[15]
1 GC	0.63 ± 0.14	4 $GC_{(AT)}$	0.23 ± 0.07
2 GC	0.58 ± 0.20	4 $GC_{(AC)}$	0.05 ± 0.02

PNA SAM assemblies that are used to measure the electrochemical charge-transfer rate constants. Oxidation and reduction peaks of ferrocene are clearly visible in voltammograms at various scan rates (see Figure 1B and Supporting Information). The voltammograms indicate that the ferrocene redox couple is quasi-reversible. The scan rate dependence of ferrocene's oxidation and reduction peaks is modeled well by Marcus theory (Figure 1C), consistent with earlier studies in ss and ds PNA.[13−16] The charge-transfer rate constants for the ds PNA SAMs appear in Table 2.

The data in Table 2 indicate that charge-transfer rate constants change when adenine-thymine (AT) bps are replaced with guanine-cytosine (GC) bps in pure 7 and 10 bp PNA, which is a clear signature of bridge mediated electron transfer. Because guanine has the lowest oxidation potential of the four nucleobases,[21] GC base pairs are expected to stabilize hole states and thus reduce the hole injection barrier and lower the tunneling barrier. For 7−10 bp PNA duplexes, prior theoretical studies[16] found that conformational fluctuations induce a mixture of superexchange and hopping hole transfer mechanisms. In this mixed-transport regime, thermal fluctuations lead to transient energy

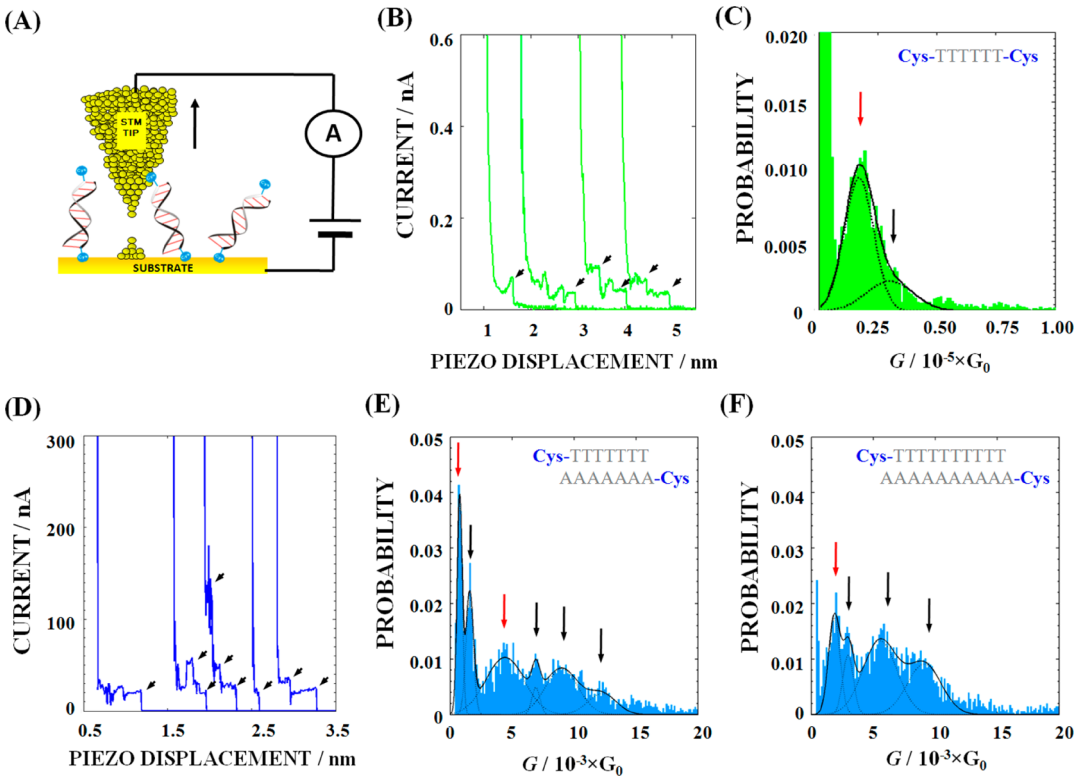

Figure 2. Results of STM-BJ measurements of single-molecule PNA conductance at a 0.4 V bias potential. Panel A shows a cartoon representation of the STM-BJ experiment. Panels B and D show current-distance profiles recorded for T_6 and 7 bp TA sequences, respectively. The plateaus indicated by black arrows correspond to the conduction through the PNA duplexes. Panels C, E, and F show probability distributions of the conductance values measured for the T_6 (C), 7 bp TA (E), and 10 bp TA (F) PNAs. The total number of counts was normalized to unity. Arrows indicate the most commonly observed conductance values. Red arrows indicate fundamental conductance values, which are attributed to the presence of a single molecule in the junction during measurement.

matching between donor and bridge states, and a GC base pair could either increase or decrease the hole transfer rate.[16] The charge-transfer rates of the mixed sequences in Table 2 reflect this complexity. Indeed, the successive addition of more than one GC base pair to either the 7 or 10 bp ds PNA sequences does not cause a significant increase in the charge-transfer rate.

The reduction in rate that is caused by base mismatches is consistent with previous observations of Barton and co-workers on the effects of a mismatch in a 15 bp DNA duplex,[25] and provides additional evidence for bridge mediated transfer. When an AC mismatch is introduced into a 10 bp PNA duplex containing 4 GC pairs, the rate of charge-transfer decreases five-fold relative to that of a 10 bp duplex with no mismatches (see Table 2, compare **10 bp 4 GC$_{(AT)}$** and **10 bp 4 GC$_{(AC)}$**).

The new data provided here and the data from our previous reports correspond to bridge-mediated charge transfer for both ss PNA and ds PNA systems, and they all use a cysteine linker group and a ferrocene reporter group.[13−16]

Single-Molecule Conductance. In single-molecule STM-BJ conductance measurements,[7] a gold STM tip acts as one electrode and a gold substrate modified with loosely packed PNA molecules is the second electrode (Figure 2A). The PNA duplexes are linked to the electrode by a cysteine (Cys) on the C-terminus. The tunneling current is measured at a constant bias voltage as a function of the distance during retraction of the tip from the substrate electrode. Whenever PNA molecules are trapped in the junction, step-like features in the current-distance profile arise from conduction through the molecules (see Figure 2B,D).

Figure 2 shows conductance distributions that are obtained by analyzing current-distance profiles for many different events. The distributions are reported for ss PNA (**T_6** in Figure 2C) and ds PNA (**7 bp TA** in Figure 2E and **10 bp TA** in Figure 2F). The distributions for the other ss thymine PNAs and ds PNAs listed in Table 1 appear in the Supporting Information. The conductance distribution for the **T_6** PNA shows one strong conductance peak with a shoulder on its high conductance side. Fitting of these data by a sum of two Gaussians provides conductance values that differ by a factor of two. The smaller conductance value, which corresponds to the maximum of the major peak in the distribution, is assigned to a single molecule in the junction. The higher conductance value, which corresponds to the maximum of the second broad peak (shoulder), is assigned to the conductance for two molecules in the junction.

TABLE 3. Single-Molecule Conductance Values *G* Measured for ss PNA by the STM-BJ Method[a]

	G/G_0		
sequence	(L)[b]	(M)[b]	(H)
T_3	$(3.0 \pm 0.8) \times 10^{-5}$	$(1.5 \pm 0.5) \times 10^{-4}$	$(3.8 \pm 1.3) \times 10^{-4}$
T_4	$(5.6 \pm 1.4) \times 10^{-6}$	$(2.9 \pm 1.3) \times 10^{-5}$	$(9.0 \pm 2.1) \times 10^{-5}$
T_5	-	$(1.8 \pm 0.5) \times 10^{-6}$	$(5.4 \pm 2.9) \times 10^{-6}$
T_6	-	-	$(1.7 \pm 0.6) \times 10^{-6}$

[a] The conductances are classified into three groups: low (L), medium (M), and high (H). [b] Because of the characteristics of the preamplifier used in the measurements of ss PNA conductance, it was not possible to resolve conductance values below 5×10^{-7} G_0 (see Methods).

The conductance distributions for the duplexes are more complicated. The conductance distribution for the **7 bp TA** displays two characteristic regions (see Figure 2E): a high probability, narrow region with *G* values between 3×10^{-4} G_0 and 2×10^{-3} G_0 and a broad region with *G* between 2×10^{-3} G_0 and 15×10^{-3} G_0. A possible explanation for this observation is the presence of molecules with two different conformations and/or contact geometries, for which the higher molecular conductance range corresponds to geometries more favorable for charge transport.[9,29−32] Each of the two regions includes several conductance peaks that are integral multiples of a fundamental conductance value. These multiples are assigned to more than one molecule trapped in the junction.[7] Only the fundamental conductance value for a single molecule trapped in the junction is used in the further analysis. The conductance distribution for the **10 bp TA** duplex shows only one region with *G* between 3×10^{-4} G_0 and 12×10^{-3} G_0. Thus, two single-molecule conductance values are assigned for the **7 bp TA** sequence and one for the **10 bp TA** sequence.

The ss PNA−T_n sequences' fundamental conductance values are shown in Table 3, and those for ds PNAs are presented in Table 4. Up to three fundamental conductance values are determined for each PNA sequence, with other peaks corresponding to their harmonics or linear combinations. Assuming that each fundamental value (marked with red arrows in Figure 2C,E,F) represents the conductance of a single molecule, the histograms suggest that no more than four molecules are present simultaneously in a junction. Following the approach of others, the different fundamental conductances, classified as low (L), medium (M), and high (H),[9] are assumed to arise from different geometries for the molecule (thiol-Au contact) in the junction. For most of the ds PNA sequences shown in Table 4, two fundamental conductance values (medium and high) are determined. For the **7 bp 1 GC** PNA, three fundamental conductance values (low, medium, and high) are identified in the Table.

TABLE 4. Single-Molecule Conductance Values *G* Measured for ds PNA Duplexes by the STM-BJ Method

		$G/10^{-3} \times G_0$		
	sequence	(L)[a]	(M)[a]	(H)
7 bp	TA	-	0.8 ± 0.2	4.4 ± 1.5
	1 GC	0.5 ± 0.1	1.8 ± 0.6	8.5 ± 0.8
	2 GC	-	1.1 ± 0.2	6.2 ± 2.2
10 bp	TA	-	-	1.9 ± 0.5
	4 $GC_{(AT)}$	-	0.8 ± 0.3	3.2 ± 0.3
	4 $GC_{(AC)}$	-	-	1.8 ± 0.5

[a] Because of the characteristics of the preamplifier used in the measurements of ds PNA conductance, it was not possible to resolve conductance values below 3×10^{-4} G_0 (see Methods); hence, only the high single-molecule conductance was observed for the less conductive sequences, such as **10 bp TA** and **10 bp 4 $GC_{(AC)}$**.

Analysis of either the high or the medium group of single-molecule conductances shows a trend similar to that observed for the electrochemical charge-transfer rates of the molecule. That is, (i) sequences containing GC base pairs have higher conductance than those built entirely of AT base pairs, and (ii) an AC mismatch lowers the conductance of a PNA duplex, which may be caused by changes in the helical base stacking of the duplex induced by the mismatch. The attenuation observed here in conductance is smaller than the attenuation reported earlier for an AC mismatch in ds DNAs.[23,24,26]

DISCUSSION

A linear relationship between the charge-transfer rate constant and the molecular conductance is not consistent with the corpus of *G* and of k^0 values described here. In the high barrier limit, the dependence of the conductance *G* and of the electrochemical rate constant k^0 on the length, *L*, of the molecular bridge can be described approximately by a decaying exponential function, namely,

$$G = G_{(L=0)} \exp[-\beta_G \times L] \quad (3)$$

and

$$k^0 = k^0_{(L=0)} \exp[-\beta_{k^0} \times L] \quad (4)$$

where $1/\beta_G$ and $1/\beta_{k^0}$ are the characteristic decay lengths (see Figures 3 and 4, and Table 5); `beta' parameters are useful to characterize the charge transport.[7−9,11,15,32−34] $G_{(L=0)}$ is the conductance at zero bridge length and $k^0_{(L=0)}$ is the rate constant at zero bridge length. Combining eqs 3 and 4, we find

$$G = [G_{(L=0)} \times (k^0_{(L=0)})^{(-\beta_G/\beta_{k^0})}] \times (k^0)^{(\beta_G/\beta_{k^0})} \quad (5)$$

A linear correlation between *G* and k^0 is expected from eq 5 only when $\beta_G = \beta_{k^0}$.

Figure 3 shows the dependence of k^0 on bridge length for alkanes,[8] ss PNA,[14,15] and ds PNA.[15] In each case, the bridge is tethered through a Au−S linkage to

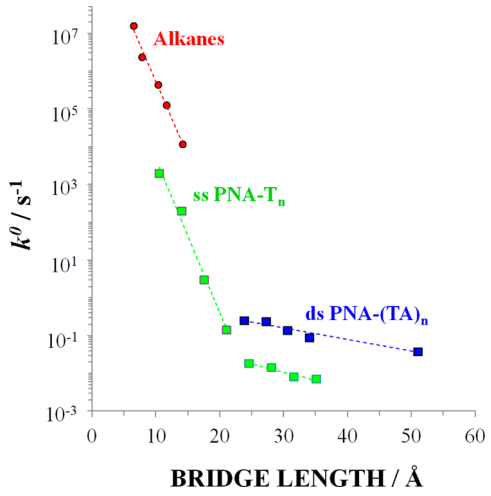

Figure 3. The electrochemical charge-transfer rate constant k^0 between a Au electrode and a ferrocene reporter group is plotted as a function of the bridge length for alkanes of `*n*' methylene groups ($n$ = 5, 6, 8, 9 and 11, red circles), ss PNA of `*n*' thymines (n = 3–10, green squares), and ds PNA of `*n*' TA base pairs (n = 7–10, 15) (dark blue squares). Data for alkanes is adapted from ref 8. Data for both ss-, and ds PNA is taken from ref 15. Dashed lines represent least-squares fits to an exponential function. Error bars are smaller than the size of the symbols. This plot demonstrates that the bridge-mediated charge-transfer rates can be described by an exponential decay, over a limited length range, for the different molecular bridges.

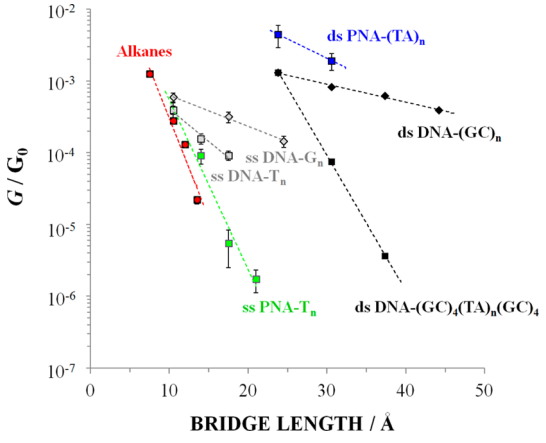

Figure 4. The single-molecule conductance *versus* the bridge length is shown for ss PNA of thymine units (ss PNA–T$_n$; n = 3–6), ds PNAs of TA base pairs (ds PNA–(AT)$_n$; n = 7, 10), alkanes (with 6, 8, 9, and 10 methylene units),[9] ss DNA of thymine (ss DNA–T$_n$; n = 3–5) or guanine (ss DNA–G$_n$; n = 3–5) nucleotides,[10] ds DNA of GC base pairs (ds DNA–(GC)$_n$; n = 8, 10, 12, 14) or with varying number of AT base pairs between GC stretches (ds DNA–(GC)$_4$(AT)$_n$(GC)$_4$; n = 0, 2, 4).[11] For clarity, only the highest conductance values (of a set of three values)[9] are shown for alkanes, ss-PNA–T$_n$, and ds-PNA–(AT)$_n$. Dashed lines represent least-squares fits to an exponential function. For DNA data, no information about the experimental error was available from the literature reports. This plot demonstrates that the molecular conductance can be described by an exponential decay, over a limited length range, for the different molecular bridges.

the electrode (cysteines for the PNAs and thiol for the alkanes) and has a ferrocene redox reporter on the opposite end of the bridge (note that the linkers were not included in the estimation of molecular bridge length, see Methods). The dashed lines represent fits of the data to eq 4. For ss PNA, the data are fit separately for short and long distance ranges. The β_{k^0} parameters are similar for short ss PNAs and alkanes.[8] This similarity, together with the fact that charge-transfer in alkanes occurs by superexchange,[8,35,36] suggests that charge-transfer in short ss PNAs also occurs *via* a superexchange mechanism in this energy regime. For ss T$_n$ PNAs with more than seven bases, and for PNA–(TA)$_n$ duplexes (with ≥7 base pairs), k^0 decreases weakly with bridge length.[15] The small values of β_{k^0} for these longer bridges (see Table 5) suggest that charge transfer in these structures occurs by hopping or by near-resonant charge transfer.[16,37–39] The change in mechanism from superexchange to hopping, which is observed during the transition from short to long T$_n$ ss PNA, is similar to that previously reported for ds DNA.[40,41] The change in mechanism can be explained by the fact that tunneling decreases exponentially with distance, while hopping drops as the inverse of the bridge length.[15]

The dependence of single-molecule conductance G on bridge length for ss PNA–T$_n$, ds PNA–(TA)$_n$, alkanes,[9] ss DNA,[10] and ds DNA[11] is presented in Figure 4. Alkane and DNA conductance data are taken from the literature and are included for comparison. The single-molecule conductance is well described by an exponential function of bridge length in all cases (because of the limited sensitivity available in our conductance measurements, we were not able to determine whether a transition to a more shallow length dependence occurs for longer chains, as observed in the electrochemical experiments). The β_G parameters for the short ss-PNA–T$_n$ and for alkanes are similar; however, these decay factors are smaller than the values found for the rate constant (see Table 5). The conductances found for ss PNA are smaller than those found for ss DNA of similar length and sequence, and the conductance of ss PNA decreases more rapidly with bridge length than is found in ss DNA. The conductances of ds-PNA–(TA)$_n$, ss DNA–G$_n$,[10] and ds DNA–(GC)$_n$[11] decay much more weakly with length than is found for ss PNA and for alkanes. Although the k^0 and G data for each molecular type are well described by functions that decay exponentially with length, the fitted β_{k^0} and β_G parameters are all different.

The single-molecule conductance measurements and the electrochemical rate experiments were performed in distinctly different settings. For example, G was measured on a single-molecule level, whereas k^0 was determined for an ensemble of molecules in closely packed self-assembled monolayers. In addition, the solvent conditions are different for the two types of measurements. While the electron tunneling is controlled by the properties of the molecular bridge, the measured electrochemical rate constant depends on

TABLE 5. The Decay Constant Values Obtained by the Least Linear Squares Exponential Fits to the k^0 and G Length Dependences and Exponent of the Power Law Fit to the $G-k^0$ Relationships

	molecular bridge	β_G (Å^{-1})	β_{k^0} (Å^{-1})	β_G/β_{k^0}	B	experimental method for determining k^0
ss PNA	T_n $n = 3-6$	(H) 0.54 ± 0.13 (M) 0.63 ± 0.20[a]	0.94 ± 0.30[14,15]	(H) 0.57 ± 0.27 (M) 0.67 ± 0.32	(H) 0.63 (M) 0.71	Cyclic voltammetry
	T_n $n = 7-10$	-	0.10 ± 0.07[15]	-	-	Cyclic voltammetry
ds PNA	Sequences listed in Table 1,[b]	N/A[d]	N/A[d]	N/A[d]	(H) 0.69 (M) 0.71	Cyclic voltammetry
	$(AT)_n$ $n = 7-10$[c]	0.12 ± 0.09	0.07 ± 0.03[15]	1.7 ± 1.3	0.82	
ss DNA	T_n $n = 3-5$	0.21 ± 0.40[10]	-	-	-	-
	G_n $n = 3-5$	0.10 ± 0.08[10]	-	-	-	-
ds DNA	$(GC)_n$ $n = 8,10,12,24$	0.06 ± 0.02[11]	-	-	-	-
	$(GC)_4(AT)_n(GC)_4$ $n = 0,2,4$	0.43 ± 0.10[11]	-	-	-	-
Alkanes	$(CH_2)_n$ $n = 6,8,9,10$	(H) 0.67 ± 0.27[9] (M) 0.70 ± 0.30[9] (L) 0.28 ± 0.36[9]	0.91 ± 0.17[8]	(H) 0.74 ± 0.33 (M) 0.77 ± 0.36 (L) 0.31 ± 0.40	(H) 0.85 (M) 0.86 (L) 0.58	indirect, laser-induced, temperature jump[8]

[a] Length dependence is provided in the Supporting Information. [b] High conductance (H) data is based on all the ds PNA sequences listed in Table 1; medium conductance (M) data is based on all 7 bp PNAs and **10 bp 4GC$_{(TA)}$** (for **10 bp TA** and **10 bp 4GC$_{(CA)}$** medium conductance was not determined; see Table. 4). [c] Conductance data is limited to **7 bp TA** and **10 bp TA** duplexes. [d] Length dependences are irrelevant.

the quality of the monolayer[14,42] and is affected by intermolecular interactions.[42−45] In addition, the molecular conductance can be affected by the solvation conditions[46−48] and local environment.[49] Therefore, the differences in the local environment of the molecules must be accounted for when comparing the experiments and drawing conclusions from them.

The electrochemical rate data on the ss PNAs[15] and alkanes[8] were shown to be bridge mediated in the original reports. The bridge-mediated character of the charge transfer in the DNA and ss PNAs is substantiated by the similar conductance values determined in different environments. For example, Van Zeling *et al.* measured similar conductances for ss and ds DNA in air and in an aqueous electrolyte.[10] We measured a very similar conductance for ss PNA in mesitylene and in aqueous electrolyte (phosphate buffer pH = 7, data not shown). Although we did not perform the measurements on the ds PNA in different environments, the bridge-mediated character of the charge transfer is evident from the length and sequence dependence of the duplexe's conductances. Tao and co-workers[29] and Wandlowski, Evers and co-workers[9] found similar conductances for the alkanedithiols in the same solvent as used in our studies (mesitylene), but with different arrangements of the molecules, specifically with the molecules randomly oriented on the surface, and with molecules in well-packed, self-assembled monolayers. These facts—the bridge-mediated nature of the charge transfer, and no distinct influence of the solvent or surface arrangement of the molecules on the measured conductance—motivated the selection of these molecules for drawing comparisons of the experimental k^0 and G values.

Figure 5 shows a plot of the single-molecule conductance G *versus* the rate constant k^0 for a subset of the systems shown in Figures 3 and 4, namely, the

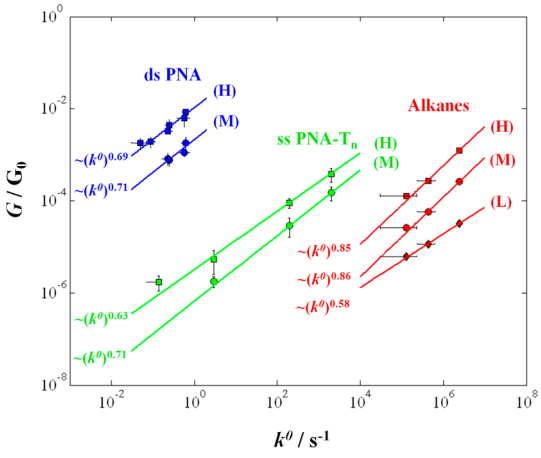

Figure 5. The single-molecule conductance G is plotted *versus* the standard electrochemical charge-transfer rate constant k^0 for alkanes (red symbols), ss PNA constructed of thymine nucleotides (ss PNA-T_n; $n = 3-6$) (green symbols), and ds PNAs (blue symbols). Lines represent the least-squares fits in the form $G = A \times (k^0)^B$, where A and B are fitting constants (see text). Electrochemical rate constant values are adapted from ref 8 for alkanes, and refs 14 and 15 for ss PNAs. Conductance values for alkanes are adapted from ref 9. The Supporting Information shows additional plots that contrast the power law fits with linear fits. Note that the same type of linker was used to attach the ss- and ds PNA molecules to the gold surface (Cys), whereas the alkyl chains are directly coupled to gold with thiol groups, rather than cysteines. While this difference may affect comparisons between the different systems (alkane *versus* PNA), it should not affect the correlation of G and k^0 for a particular molecular bridge.

alkane, ss PNA, and ds PNA bridges. These systems are selected because the electrochemical rates and conductances for these bridges were measured with the same linker groups and the same redox reporter. Good least-squares fits by a power law, $G = A \times (k^0)^B$, are found for B values in the range 0.58−0.86. For alkanes and ss PNA, the fitted B values are in good agreement

with the β_G/β_{k^0} ratios obtained from the length dependences of k^0 and of G (see Table 5). For ds PNA, the power law exponent B is smaller than the β_G/β_{k^0} value obtained from the length dependence data (see Table 5); however, the smaller β values have a larger relative error and this difference may not be significant. Overall, the nonlinearity of the $G-k^0$ relationship correlates with differences in the distance dependences of $k^0(L)$ (measured using electrochemistry) and $G(L)$ (measured with STM break junctions). Below, we discuss the charge-transport parameters and the underlying mechanisms that can create these differences in the distance dependence of charge-transfer rates and conductances.

Previous theoretical studies,[2−5] which relate unimolecular, electrochemical, and break-junction measurements and suggest a linear rate-conductance relationship, assume that (i) the tunneling/charge-transfer barriers are the same for the different experiments on the same bridges, (ii) the charge-transfer mechanism is either pure superexchange or pure hopping, and (iii) either no dephasing occurs (pure superexchange) or complete dephasing occurs (pure incoherent hopping). Does relaxing any of these assumptions lead to differences in the distance dependence of charge-transfer rates and molecular conductance, thus explaining the observed nonlinearity of the rate-conductance relationships? Indeed, all models of coherent charge transfer indicate that lower tunneling barriers produce a softer distance dependence and lower β values.[50] As the distance decay softens with bridge length, charge transport occurs by a mixture of coherent and incoherent mechanisms. For superexchange or hopping transport, the distance dependencies are very sensitive to the charge tunneling or injection barriers. In particular, the observed rate-conductance power law with $\beta_G/\beta_{k^0} < 1$ can be explained if the energy barrier for charge transport is lower in experiments that measure conductances *versus* those that measure rates.

What underlying factors could produce such differences in energy barriers for the same chemical bridges? Polarization of the electrodes when charges are injected into a molecular bridge creates a stabilizing image charge.[51,52] The work function of the electrodes in the STM-BJ experiments and the redox potentials of the charge donor/acceptors in electrochemical experiments need not be equal, leading to different barriers for both charge tunneling and injection in the two cases. The solvation environment for molecular bridges in the electrochemical experiments (dense monolayers) differs from that in the STM-BJ experiments (sparse monolayers with molecules close to solution). Finally, in molecular junctions, charging of the molecular bridge as well as the molecule-metal contact is possible. All of these effects can lead to different charge transport energy barriers. In our analysis, as in the earlier studies, we are comparing transport through the same chemical bridges. We are developing a theoretical model to account for these effects and it reveals that system dependent energy barriers and dephasing, arising from the interaction of the electronic states of the bridge with the solvent environment, influence the distance dependence of rates and conductances (*vide infra*).

Breakdown in the Correlation between *G* and k^0 among Different Chemical Species. A power law correlation between G and k^0 is found for each of the molecular bridge types: alkanes, ss PNA, and ds PNA (see Figure 5). When the data for all three species are considered together as a single data set, however, the $G-k^0$ correlation is lost. For example, the ds PNAs have the smaller electrochemical rates, but they have the highest conductances, relative to most of the ss PNA sequences. Can this loss of correlation be understood in terms of changes in the nature of the molecule-electrode coupling in the electrochemical and STM-BJ experiments? The experimental design used in this study compares molecules with the same linker group (cysteine for the PNA and thiol for the alkane) to minimize differences arising from the molecule-electrode contact. The different conductance groups (H, M, and L) in Tables 3 and 4 are attributed to different types of electrode contact geometries for the molecular bridges. From the analysis (see Table 5), it is clear that each of the conductance groups displays a power law correlation but the absolute values of the conductance are shifted with respect to each other (see Figure 5); however, these shifts are less than a factor of 10, whereas the shift between the ss PNA and the ds PNA is 10 000 times. To explain the differences in the conductance *versus* rate constant correlation, one would need to require that the duplex PNA has a dramatically stronger Au-cysteine contact than does the ss PNA in the conductance measurements, but that they have similar Au−cysteine contacts in the electrochemical measurements. Given that two conductance groups can be identified for ss PNA and ds PNA and that their features are similar to those found for other thiol−Au systems that have been studied by the STM-BJ method,[9] it seems improbable that the electrode-molecule linkage accounts for the entire shift in conductance (see Figure 5).

The lack of correlation between G and k^0 among different chemical species may arise from different charge-transfer regimes being operative (*e.g.*, superexchange in alkanes *versus* near resonant charge-transfer or hopping in ds PNA). Consequently, we anticipate that the local molecular environment (bath interactions) may affect the charge transport differently; bath interactions influence both the charge-transfer barrier and electronic dephasing (loss of wave function coherence arising from local fluctuations of the environment/bath). The effect of dephasing on the transport is more subtle than barrier height effects. For hopping transport, an increase in the dephasing rate

increases the resistance to charge transport because of the increased probability to backscatter the charge. In contrast, an increased dephasing rate broadens the bridge energy eigenvalues and thus enhances the charge-transfer rate in the superexchange limit. Previous theoretical studies have found that dephasing also affects the distance dependence of charge-transfer kinetics. For example, dephasing effects can make charge-transfer rates nearly distance independent for long bridges.[53,54] Previous work showed that dephasing can differentially alter charge transfer rates for ds PNA molecular bridges with different sequences.[16] Thus, modification of energy barrier heights or of dephasing rates can produce distinctive distance dependences for very similar structures (compare Figures 3 and 4). A more quantitative analysis of dephasing and energy barriers effects on charge transfer is described in a forthcoming paper.

CONCLUSIONS

This study explores the relationship between electrochemical charge-transfer rates and molecular conductances for alkanes, ss PNA, and ds PNA. A (nonlinear) power law relationship was found between the electrochemical rate constants and the single-molecule conductances for each of the three molecular bridge species. A loss of correlation between molecular conductance and charge-transfer rates is found when considering these data as a whole. In fact, the ds PNA data exhibit the slowest charge-transfer rates and the largest molecular conductances of the three molecular-bridge species. We associate the source of the nonlinear relation between the rates and conductances with differences in (i) charge-transfer energy barriers (*i.e.*, the energy gap between charge-carrying states on the bridge and those on the donor/acceptor/electrode), and (ii) bridge dephasing in the two experimental configurations. In situations where multiple mechanisms of charge transport are possible, as in the case of the bridges discussed here, changes in charge-transfer energy barriers and bridge dephasing can lead to differences between the distance dependence of the charge-transfer rates and the conductances. Thus, the relative propensity of different chemical species to transmit charge, as deduced from electrochemical measurements and from molecular junction studies, may not be the same.

METHODS

PNA Synthesis. The synthesis of PNA oligomers with C-terminal cysteine and N-terminal ferrocene moieties was performed using solid phase peptide synthesis methods with a Boc protection strategy,[55−57] as reported in earlier studies.[13,14] MBHA resin (Peptides International, Louisville, KY) with a loading of 0.18 mequiv/g was down-loaded[57] using Boc-L-Cys-(4-MeOBzl)-OH (NovaBiochem/Merck Biosciences, Switzerland) to an estimated loading of 0.04−0.06 mequiv/g. Thereafter, depending on sequence, Boc-T-OH/Boc-(A-Z)-OH/Boc-(G-Z)-OH/Boc-(C-Z)-OH (Applied Biosystems, Foster City, CA) or *N*-(2-Boc-aminoethyl)-*N*-(methyl)-glycine were coupled using 1*H*-benzotriazolium 1-[*bis*(dimethylamino)methylene]-5chloro-hexafluorophosphate(1),3-oxide (HCTU) (Peptides International) as a coupling agent. Finally, ferrocene carboxylic acid (Aldrich) was coupled to the N-terminus. This coupling was repeated twice to increase the yield of ferrocene-conjugated PNA. Oligomers were cleaved from the resin using trifluoroacetic acid (TFA) and trifluoromethanesulfonic acid (TFMSA), precipitated in ethyl ether, and dried under nitrogen. PNA was purified by reversed-phase HPLC using a C18 silica column on a Waters 600 instrument. Absorbance was measured at 260 nm with a Waters 2996 Photodiode Array Detector. Characterization of the oligomers was performed by MALDI-ToF mass spectrometry on an Applied Biosystems Voyager Biospectrometry Workstation with Delayed Extraction and an *R*-cyano-4-hydroxycinnamic acid matrix (10 mg/mL in 1:1 water/acetonitrile, 0.1% TFA). PNA solutions were prepared in deionized water, and the PNA concentrations were determined by UV−vis spectrophotometry assuming $\varepsilon(260)$ = 8600, 6600, 13 700, and 11 700 cm^{-1} M^{-1} for each T, C, A, and G monomer, respectively.[57] PNA solutions for electrode incubation were typically 20 μM ss-PNA in 1:1 (v/v) acetonitrile/20 mM pH 7.0 sodium phosphate buffer. *m/z* for $(M + H)^+$ were calculated and found to be Cys-T_3-Cys 1022/1024, Cys-T_4-Cys 1288/1290, Cys-T_5-Cys 1555/1556, Cys-T_6-Cys 1821/1822, Cys-T_7 1984/1986, Cy-A_7 2047/2050, Cys-TTTGTTT 2009/2010, Cys-AAACAAA 2023/2024, Cys-AAGTTGT 2052/2054, Cys-ACAACTT 1981/1983, Cys-T_{10} 2783/2785, Cys-A_{10} 2873/2873, Cys-TCACTAGATG 2830/2831, Cys-CATCTAGTGA 2830/2830, Cys-CATCCAGTGA 2815/2816. The mass spectrometry data are reported for Cys-T_n-Fc in ref 15, and for the strands used for synthesis of ferrocenated PNA duplexes: **10 bp TA** in ref 15, **7 bp TA**, **7 bp 1 GC** and **7 bp 2 GC** in ref 16, **10 bp 4 GC$_{(AT)}$** and **10 bp 4 GC$_{(AC)}$** in ref 28.

Electrochemical Characterization of PNA SAMs. Gold ball electrodes were prepared using the annealing procedure described earlier.[13−16] To summarize, 20 μM ds PNA solutions were prepared in 1:1 (v/v) acetonitrile, pH 7.0/20 mM sodium phosphate buffer, and annealed in solution by heating at 90 °C for 10 min, followed by slow (∼2 h) cooling to room temperature, in order to ensure duplex formation. The electrodes were then coated with PNA SAMs by immersion in the ds PNA solutions at 27 °C for 28−40 h. Following incubation, electrodes were washed with deionized water and used directly in electrochemical experiments. Cyclic voltammetry was performed using a CH Instruments 618B or CHI430 electrochemical analyzer. The electrochemical cell was comprised of a Ag/AgCl (1 M KCl) reference electrode, a platinum wire counter electrode, and a PNA-modified gold wire electrode immersed in a 1 M $NaClO_4$ (pH ≈ 6−7) solution. Kinetic data were obtained by plotting the peak separation *versus* scan rate and fitting the data by Marcus theory[43,58] with a reorganization energy (λ) of 0.8 eV.[43]

Single-Molecule Conductance (STM-Controlled Break Junction) Measurements. All measurements were performed with an Agilent 5500 system with an environmental chamber. The STM head was housed in a homemade acoustically isolated Faraday cage and placed on an active antivibrational system (Table Stable) on an optical table (*vide infra*). The STM-BJ technique[7] is described in the Supporting Information.

Sample Preparation. Gold films on mica (Agilent Technologies, Inc.) were coated with PNA molecules through cysteine linkages. For the ss PNA samples, the electrode was immersed in a 20 μM solution (1:1 mixture by volume of water and acetonitrile) for 30 min at room temperature, which formed a loosely packed layer of molecules. For the ds PNA samples, the ds PNA was first hybridized by heating a mixture of complementary strands at 90 °C for ∼10 min, followed by slow (∼2 h) cooling to room temperature. Subsequently, the electrode was immersed in this solution for 30 min at room temperature to form a loosely packed film. In all cases, the PNA-modified

substrates were rinsed with ethanol and dried under an argon gas stream prior to further experiments.

Conductance Measurements. The molecular conductance of the ss and ds PNA was measured using the STM-controlled break-junction method.[7] In this method, the molecules of interest are occasionally trapped between the gold substrate and an STM tip by periodic modulation of the tip−substrate separation. The tunneling current is monitored as a function of the tip−substrate distance under a constant bias voltage. When a molecule is trapped in the junction, the current *versus* displacement curve has step-like features; *i.e.,* it deviates from an exponential distance dependence (see Figure 2B,D). The conductance is calculated from these current plateaus and the applied bias for each event.[7]

Experiments were performed using freshly cut gold STM tips (0.25 mm, 99.999% gold wire, Alfa Aesar). Typically, 5−10 tips were used to collect sufficient data for a single PNA sequence. All experiments were performed in bicyclohexyl in an argon atmosphere. In the case of ss PNA, a 0.4 V bias voltage and a 10 nA/V preamplifier were used in the measurements. Curves with current plateaus were selected manually for further analysis. ds PNA molecules were measured with a 0.4 V bias voltage and a logarithmic preamplifier, which was limited to the 10 nA to 22 μA range. A semiautomated filtering procedure (see Supporting Information) was performed to select current-distance profiles with step-like features. These selected curves (1−2% of the total data set) were inspected to reject unusually noisy data. For both ss- and ds PNA, measurements were performed on at least three independently prepared samples, resulting in the collection of 20 000−30 000 current-distance profiles for each type of PNA duplex. Measured conductances were plotted in the form of normalized histograms, which were then fit by a sum of Gaussian functions to assist in locating the conductance peaks. All conductance results are expressed in units of $G_0 = 2e^2/h \approx 77\ \mu S$, the quantum of conductance.

Molecular Bridge Length Calculations. End groups (thiol terminal groups, cysteines, and ferrocene redox probes) were not included in the calculation of the length of the molecular bridges. Values of 1.28 Å per methylene unit, 3.5 Å per base, and 3.4 Å per base pair were used to calculate the total length of the alkyl, ss nucleic acids, and ds nucleic acids molecular bridges, respectively.

Conflict of Interest: The authors declare no competing financial interest.

Acknowledgment. The authors gratefully acknowledge support from the National Science Foundation (CHE 1057953 to D.N.B., CHE 0809838 to E.B., CHE 1059037 to C.A., and CHE 1057981 to D.H.W.). K.L.D. acknowledges support from a Goldblatt Fellowship during part of this research.

Supporting Information Available: Additional cyclic voltammogramms and Marcus theory fits are provided. Details of the single-molecule conductance measurements, and procedures for filtering of the data are provided. Conductance distributions for ss and ds PNAs and dependencies of low and medium classes of conductance on the length of ss-PNA are included. Linear and power law fits to rate constant-conductance data and calculated parameters of the $G-k^0$ fits are provided. This material is available free of charge *via* the Internet at http://pubs.acs.org.

REFERENCES AND NOTES

1. Onuchic, J. N.; Beratan, D. N.; Hopfield, J. J. Some Aspects of Electron-Transfer Reaction Dynamics. *J. Phys. Chem.* **1986**, *90*, 3707–3721.
2. Nitzan, A. A Relationship between Electron-Transfer Rates and Molecular Conduction. *J. Phys. Chem. A* **2001**, *105*, 2677–2679.
3. Nitzan, A. The Relationship between Electron Transfer Rate and Molecular Conduction 2. The Sequential Hopping Case. *Isr. J. Chem.* **2002**, *42*, 163–166.
4. Berlin, Y. A.; Ratner, M. A. Intra-Molecular Electron Transfer and Electric Conductance *via* Sequential Hopping: Unified Theoretical Description. *Radiat. Phys. Chem.* **2005**, *74*, 124–131.
5. Traub, M. C.; Brunschwig, B. S.; Lewis, N. S. Relationships between Nonadiabatic Bridged Intramolecular, Electrochemical, and Electrical Electron-Transfer Processes. *J. Phys. Chem. B* **2007**, *111*, 6676–6683.
6. Zhou, X.-S.; Liu, L.; Fortgang, P.; Lefevre, A.-S.; Serra-Muns, A.; Raouafi, N.; Amatore, C.; Mao, B.-W.; Maisonhaute, E.; Schoellhorn, B. Do Molecular Conductances Correlate with Electrochemical Rate Constants? Experimental Insights. *J. Am. Chem. Soc.* **2011**, *133*, 7509–7516.
7. Xu, B.; Tao, N. J. Measurement of Single-Molecule Resistance by Repeated Formation of Molecular Junctions. *Science* **2003**, *301*, 1221–1223.
8. Smalley, J. F.; Finklea, H. O.; Chidsey, C. E. D.; Linford, M. R.; Creager, S. E.; Ferraris, J. P.; Chalfant, K.; Zawodzinsk, T.; Feldberg, S. W.; Newton, M. D. Heterogeneous Electron-Transfer Kinetics for Ruthenium and Ferrocene Redox Moieties through Alkanethiol Monolayers on Gold. *J. Am. Chem. Soc.* **2003**, *125*, 2004–2013.
9. Li, C.; Pobelov, I.; Wandlowski, T.; Bagrets, A.; Arnold, A.; Evers, F. Charge Transport in Single Au | Alkanedithiol | Au Junctions: Coordination Geometries and Conformational Degrees of Freedom. *J. Am. Chem. Soc.* **2007**, *130*, 318–326.
10. van Zalinge, H.; Schiffrin, D. J.; Bates, A. D.; Haiss, W.; Ulstrup, J.; Nichols, R. J. Single-Molecule Conductance Measurements of Single- and Double-Stranded DNA Oligonucleotides. *ChemPhysChem* **2006**, *7*, 94–98.
11. Xu, B.; Zhang, P. M.; Li, X. L.; Tao, N. J. Direct Conductance Measurement of Single DNA Molecules in Aqueous Solution. *Nano Lett.* **2004**, *4*, 1105–1108.
12. Venkatramani, R.; Keinan, S.; Balaeff, A.; Beratan, D. N. Nucleic Acid ChargeTransfer: Black, White and Gray. *Coord. Chem. Rev.* **2011**, *255*, 635–648.
13. Paul, A.; Bezer, S.; Venkatramani, R.; Kocsis, L.; Wierzbinski, E.; Balaeff, A.; Keinan, S.; Beratan, D. N.; Achim, C.; Waldeck, D. H. Role of Nucleobase Energetics and Nucleobase Interactions in Single-Stranded Peptide Nucleic Acid Charge Transfer. *J. Am. Chem. Soc.* **2009**, *131*, 6498–6507.
14. Paul, A.; Watson, R. M.; Lund, P.; Xing, Y.; Burke, K.; He, Y.; Borguet, E.; Achim, C.; Waldeck, D. H. Charge Transfer through Single-Stranded Peptide Nucleic Acid Composed of Thymine Nucleotides. *J. Phys. Chem. C* **2008**, *112*, 7233–7240.
15. Paul, A.; Watson, R. M.; Wierzbinski, E.; Davis, K. L.; Sha, A.; Achim, C.; Waldeck, D. H. Distance Dependence of the Charge Transfer Rate for Peptide Nucleic Acid Monolayers. *J. Phys. Chem. B* **2010**, *114*, 14140–14148.
16. Venkatramani, R.; Davis, K. L.; Wierzbinski, E.; Bezer, S.; Balaeff, A.; Keinan, S.; Paul, A.; Kocsis, L.; Beratan, D. N.; Achim, C.; Waldeck, D. H. Evidence for a Near-Resonant Charge Transfer Mechanism for Double-Stranded Peptide Nucleic Acid. *J. Am. Chem. Soc.* **2011**, *133*, 62–72.
17. Iqbal, S. M.; Balasundaram, G.; Ghosh, S.; Bergstrom, D. E.; Bashir, R. Direct Current Electrical Characterization of ds-DNA in Nanogap Junctions. *Appl. Phys. Lett.* **2005**, *86*, 153901–3.
18. Kawai, K.; Kodera, H.; Majima, T. Long-Range Charge Transfer through DNA by Replacing Adenine with Diaminopurine. *J. Am. Chem. Soc.* **2009**, *132*, 627–630.
19. Kawai, K.; Kodera, H.; Osakada, Y.; Majima, T. Sequence-Independent and Rapid Long-Range Charge Transfer through DNA. *Nat. Chem.* **2009**, *1*, 156–159.
20. Nogues, C.; Cohen, S. R.; Daube, S.; Apter, N.; Naaman, R. Sequence Dependence of Charge Transport Properties of DNA. *J. Phys. Chem. B* **2006**, *110*, 8910–8913.
21. Seidel, C. A. M.; Schulz, A.; Sauer, M. H. M. Nucleobase-Specific Quenching of Fluorescent Dyes. 1. Nucleobase One-Electron Redox Potentials and Their Correlation with Static and Dynamic Quenching Efficiencies. *J. Phys. Chem.* **1996**, *100*, 5541–5553.
22. Treadway, C. R.; Hill, M. G.; Barton, J. K. Charge Transport through a Molecular [pi]-Stack: Double Helical DNA. *Chem. Phys.* **2002**, *281*, 409–428.
23. Hihath, J.; Xu, B.; Zhang, P. M.; Tao, N. J. Study of Single-Nucleotide Polymorphisms by Means of Electrical

Conductance Measurements. *Proc. Natl. Acad. Sci. U.S.A.* **2005**, *102*, 16979–16983.
24. Guo, X.; Gorodetsky, A. A.; Hone, J.; Barton, J. K.; Nuckolls, C. Conductivity of a Single DNA Duplex Bridging a Carbon Nanotube Gap. *Nat. Nanotechnol.* **2008**, *3*, 163–167.
25. Kelley, S. O.; Jackson, N. M.; Hill, M. G.; Barton, J. K. Long-Range Electron Transfer through DNA Films. *Angew. Chem., Int. Ed.* **1999**, *38*, 941–945.
26. Wierzbinski, E.; Arndt, J.; Hammond, W.; Slowinski, K. *In Situ* Electrochemical Distance Tunneling Spectroscopy of ds-DNA Molecules. *Langmuir* **2006**, *22*, 2426–2429.
27. Boal, A. K.; Barton, J. K. Electrochemical Detection of Lesions in DNA. *Bioconjugate Chem.* **2005**, *16*, 312–321.
28. Wierzbinski, E.; de Leon, A.; Davis, K. L.; Bezer, S.; Wolak, M. A.; Kofke, M. J.; Schlaf, R.; Achim, C.; Waldeck, D. H. Charge Transfer through Modified Peptide Nucleic Acids. *Langmuir* **2012**, *28*, 1971–1981.
29. Li, X.; He, J.; Hihath, J.; Xu, B.; Lindsay, S. M.; Tao, N. J. Conductance of Single Alkanedithiols: Conduction Mechanism and Effect of Molecule-Electrode Contacts. *J. Am. Chem. Soc.* **2006**, *128*, 2135–2141.
30. Martin, S.; Giustiniano, F.; Haiss, W.; Higgins, S. J.; Whitby, R. J.; Nichols, R. J. Influence of Conformational Flexibility on Single-Molecule Conductance in Nano-Electrical Junctions. *J. Phys. Chem. C* **2009**, *113*, 18884–18890.
31. Omori, Y.; Tobita, J.; Kato, Y.; Akiba, U.; Fujihira, M. Three Contact Modes of Amino Terminal Groups on Gold in Single Molecular Junction of Au/1,4-Diaminobutane/Au. *Jap. J. App. Phys.* **2007**, *46*, 7829–7837.
32. Wierzbinski, E.; Slowinski, K. *In Situ* Wiring of Single Molecules into an Electrical Circuit *via* Electrochemical Distance Tunneling Spectroscopy. *Langmuir* **2006**, *22*, 5205–5208.
33. Sek, S.; Misicka, A.; Swiatek, K.; Maicka, E. Conductance of Alpha-Helical Peptides Trapped within Molecular Junctions. *J. Phys. Chem. B* **2006**, *110*, 19671–19677.
34. Berlin, Y. A.; Burin, A. L.; Ratner, M. A. Charge Hopping in DNA. *J. Am. Chem. Soc.* **2000**, *123*, 260–268.
35. Slowinski, K.; Chamberlain, R. V.; Bilewicz, R.; Majda, M. Evidence for Inefficient Chain-to-Chain Coupling in Electron Tunneling through Liquid Alkanethiol Monolayer Films on Mercury. *J. Am. Chem. Soc.* **1996**, *118*, 4709–4710.
36. Slowinski, K.; Chamberlain, R. V.; Miller, C. J.; Majda, M. Through-Bond and Chain-to-Chain Coupling. Two Pathways in Electron Tunneling through Liquid Alkanethiol Monolayers on Mercury Electrodes. *J. Am. Chem. Soc.* **1997**, *119*, 11910–11919.
37. Xing, Y.; Park, T.-H.; Venkatramani, R.; Keinan, S.; Beratan, D. N.; Therien, M. J.; Borguet, E. Optimizing Single-Molecule Conductivity of Conjugated Organic Oligomers with Carbodithioate Linkers. *J. Am. Chem. Soc.* **2010**, *132*, 7946–7956.
38. Lu, Q.; Liu, K.; Zhang, H.; Du, Z.; Wang, X.; Wang, F. From Tunneling to Hopping: A Comprehensive Investigation of Charge Transport Mechanism in Molecular Junctions Based on Oligo(*p*-phenylene ethynylene)s. *ACS Nano* **2009**, *3*, 3861–3868.
39. Malak, R. A.; Gao, Z.; Wishart, J. F.; Isied, S. S. Long-Range Electron Transfer Across Peptide Bridges: The Transition from Electron Superexchange to Hopping. *J. Am. Chem. Soc.* **2004**, *126*, 13888–13889.
40. Giese, B.; Amaudrut, J.; Kohler, A. K.; Spormann, M.; Wessely, S. Direct Observation of Hole Transfer through DNA by Hopping between Adenine Bases and by Tunnelling. *Nature* **2001**, *412*, 318–320.
41. Lewis, F. D.; Zhu, H.; Daublain, P.; Fiebig, T.; Raytchev, M.; Wang, Q.; Shafirovich, V. Crossover from Superexchange to Hopping as the Mechanism for Photoinduced Charge Transfer in DNA Hairpin Conjugates. *J. Am. Chem. Soc.* **2005**, *128*, 791–800.
42. Chidsey, C. E. D.; Bertozzi, C. R.; Putvinski, T. M.; Mujsce, A. M. Coadsorption of Ferrocene-Terminated and Unsubstituted Alkanethiols on Gold: Electroactive Self-Assembled Monolayers. *J. Am. Chem. Soc.* **1990**, *112*, 4301–4306.
43. Napper, A. M.; Liu, H.; Waldeck, D. H. The Nature of Electronic Coupling between Ferrocene and Gold through Alkanethiolate Monolayers on Electrodes: The Importance of Chain Composition, Interchain Coupling, and Quantum Interference. *J. Phys. Chem. B* **2001**, *105*, 7699–7707.
44. Sek, S.; Misicka, A.; Bilewicz, R. Effect of Interchain Hydrogen Bonding on Electron Transfer through Alkanethiol Monolayers Containing Amide Bonds. *J. Phys. Chem. B* **2000**, *104*, 5399–5402.
45. Wain, A. J.; Do, H. N. L.; Mandal, H. S.; Kraatz, H.-B.; Zhou, F. Influence of Molecular Dipole Moment on the Redox-Induced Reorganization of α-Helical Peptide Self-Assembled Monolayers: An Electrochemical SPR Investigation. *J. Phys. Chem. C* **2008**, *112*, 14513–14519.
46. Leary, E.; Hoebenreich, H.; Higgins, S. J.; van Zalinge, H.; Haiss, W.; Nichols, R. J.; Finch, C. M.; Grace, I.; Lambert, C. J.; McGrath, R.; *et al.* Single-Molecule Solvation-Shell Sensing. *Phys. Rev. Lett.* **2009**, *102*, 086801.
47. Li, X.; Hihath, J.; Chen, F.; Masuda, T.; Zang, L.; Tao, N. Thermally Activated Electron Transport in Single Redox Molecules. *J. Am. Chem. Soc.* **2007**, *129*, 11535–11542.
48. Cao, H.; Jiang, J.; Ma, J.; Luo, Y. Temperature-Dependent Statistical Behavior of Single Molecular Conductance in Aqueous Solution. *J. Am. Chem. Soc.* **2008**, *130*, 6674–6675.
49. Selzer, Y.; Cai, L.; Cabassi, M. A.; Yao, Y.; Tour, J. M.; Mayer, T. S.; Allara, D. L. Effect of Local Environment on Molecular Conduction: Isolated Molecule *versus* Self-Assembled Monolayer. *Nano Lett.* **2005**, *5*, 61–65.
50. Simmons, J. G. Generalized Formula for the Electric Tunnel Effect between Similar Electrodes Separated by a Thin Insulating Film. *J. Appl. Phys.* **1963**, *34*, 1793–1803.
51. Kubatkin, S.; Danilov, A.; Hjort, M.; Cornil, J.; Bredas, J. L.; Stuhr-Hansen, N.; Hedegard, P.; Bjornholm, T. Single-Electron Transistor of a Single Organic Molecule with Access to Several Redox States. *Nature* **2003**, *425*, 698–701.
52. B., N. J.; Hybertson, M. S.; Louie, S. G. Renormalization of Molecular Electronic Levels at Metal-Molecule Interfaces. *Phys. Rev. Lett.* **2006**, *97*, 216405.
53. Felts, A. K.; Pollard, W. T.; Friesner, R. A. Multilevel Redfield Treatment of Bridge-Mediated Long-Range Electron Transfer: A Mechanism for Anomalous Distance Dependence. *J. Phys. Chem.* **1995**, *99*, 2929–2940.
54. Davis, W. B.; Wasielewski, M. R.; Ratner, M. A.; Mujica, V.; Nitzan, A. Electron Transfer Rates in Bridged Molecular Systems: A Phenomenological Approach to Relaxation. *J. Phys. Chem. A* **1997**, *101*, 6158–6164.
55. Anderson, G. W.; McGregor, A. C. *t*-Butyloxycarbonylamino Acids and Their Use in Peptide Synthesis. *J. Am. Chem. Soc.* **1957**, *79*, 6180–6183.
56. McKay, F. C.; Albertson, N. F. New Amine-masking Groups for Peptide Synthesis. *J. Am. Chem. Soc.* **1957**, *79*, 4686–4690.
57. Nielsen, P. E. *Peptide Nucleic Acids: Protocols and Applications*; Horizon Bioscience: Wyndmondham, 2004.
58. Weber, K.; Creager, S. E. Voltammetry of Redox-Active Groups Irreversibly Adsorbed onto Electrodes. Treatment Using the Marcus Relation between Rate and Overpotential. *Anal. Chem.* **1994**, *66*, 3164–3172.